Advanced Rigid Ablative Thermal Protection Systems

J.D. Feldman*
ERC Inc. at NASA Ames Research Center, Moffett Field, CA 94035-1000

M.J. Gasch†
NASA Ames Research Center, Moffett Field, CA 94035-1000

C.C. Poteet‡
NASA Langley Research Center, Hampton, VA 23681-2199

Christine Szalai§
Jet Propulsion Laboratory, California Institute of Technology, Pasadena, CA 91109

With the gradual increase in robotic rover sophistication and the desire for humans to explore the solar system, the need for reentry systems to deliver large payloads into planetary atmospheres is looming. Heritage ablative Thermal Protection Systems (TPS) using Viking or Pathfinder era materials are at or near their performance limits and will be inadequate for many future missions. Significant advances in TPS materials technology are needed in order to enable subsequent human exploration missions. This paper summarizes some recent progress at NASA in developing families of advanced rigid ablative TPS that could be used for thermal protection in planetary entry missions. In particular, the effort focuses on technologies required to land heavy masses on Mars to facilitate exploration.

Nomenclature

α	= Thermal diffusivity
Cp	= Specific Heat Capacity
k	= Thermal conductivity
ρ	= Density

I. Introduction

In 2009 the Exploration Technology Development Program established the Entry, Descent and Landing Technology Development Project (EDL TDP), to be managed programmatically at Langley Research Center (LaRC) and technically at Ames Research Center (ARC). The purpose of the project was to further the technologies required to land heavy (~40 metric ton) masses on Mars to facilitate exploration. The EDL Systems Analysis team studied nine system architectures for delivering heavy payloads to the Martian surface and concluded that many of the technologies needed were underdeveloped or did not exist.[1-2] The EDL architectures relied on either a mid L/D (Lift/Drag) aeroshell, a large diameter deployable decelerator, supersonic retropropulsion, or combinations of all three technologies.

---

* Materials Engineer, Thermal Protection Materials Branch, MS 223-3. Member AIAA.
† Materials Engineer, Thermal Protection Materials Branch, MS 234-1. Member AIAA.
‡ Aerospace Engineer, Structural Mechanics and Concepts Branch, MS 190.
§ Senior Systems Engineer, EDL Systems and Advanced Technologies MS 301-490. Member AIAA.

The EDL TDP contains three technical elements. They are:

1) Thermal Protection Systems (TPS) development
2) Modeling and Tools (MAT) development
3) Supersonic Retropropulsion (SRP) development

The primary goals of the EDL TDP TPS element are to design and develop TPS materials capable of withstanding the severe aerothermal loads associated with aerocapture and entry into the Martian atmosphere while significantly decreasing the TPS mass fraction contribution to the entry system. Significant advancements in TPS materials technology are needed in order to enable heavy mass payloads delivery to the Martian surface for robotic precursor and subsequent human exploration missions.

The EDL TDP TPS element is further divided into two different TPS concepts for Mars EDL, those being:

- Rigid TPS for a mid L/D aeroshell (10 meter diameter, 30 meter length)
- Flexible TPS for a large diameter deployable aerodynamic decelerator (> 20 meter diameter)

This paper focuses on the screening and development of the Rigid TPS concepts investigated under the EDL TDP. The rigid aeroshell TPS concept is required to survive two heating pulses, the first during aerocapture into Mars orbit, and the second during entry into the Mars atmosphere for descent and landing onto the Mars surface. In addition, this rigid aeroshell TPS concept is required to minimize TPS mass in order to maximize payload mass. The aerocapture and entry phases could be separated by as much as six months. The mid L/D concept consists of an approximately 10 meter diameter by 30 meter long body with three general regions of thermal heating: the backshell (lowest heating), nose cone (mid heating), and heatshield (highest heating). Figure 1 depicts the mid L/D rigid aeroshell TPS concept. The work in this paper focuses only on the windward side heatshield of the mid L/D body, where the highest heating will occur. Examples of TPS concepts tested by the NASA project team for the rigid aeroshell application include multilayer (e.g., ablator over insulator or ablator over ablator) and conformable systems. Non-tiled TPS concepts were strongly preferred.

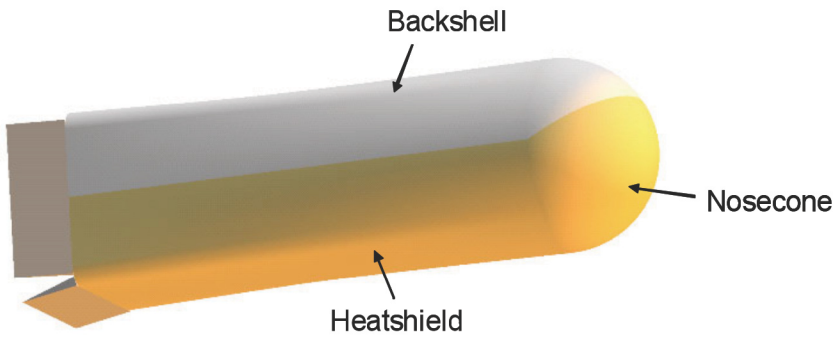

Figure 1. Mid L/D rigid aeroshell TPS concept.

Upon arrival at Mars via a trans-Mars injection from Low Earth Orbit, the mid L/D vehicle undergoes an aerocapture maneuver to both reduce the vehicle velocity and bring it into Mars orbit. Estimated heating rates for the aerocapture maneuver are shown in Table 1. Once in Mars orbit (up to six months), the mid L/D vehicle will then enter the Mars atmosphere at hypersonic velocities, and the heatshield will be jettisoned at approximately Mach 5. Table 1 shows the estimated peak entry environments, and Figure 2 shows the heating profiles for the aerocapture and entry.

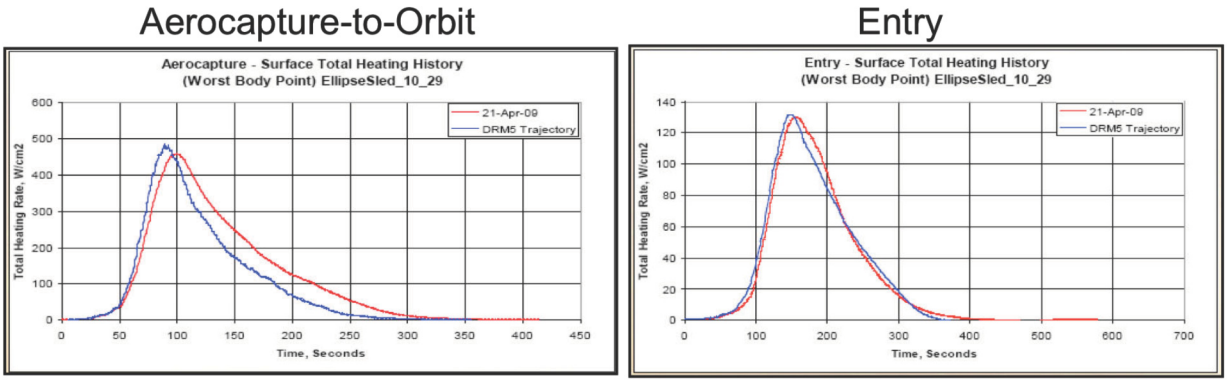

Figure 2. Heat time profiles for mid-L/D aeroshell.

Table 1. Peak aerothermal entry environments for mid L/D rigid aeroshell.

Aerothermal Entry Environments-Rigid	
Peak Heat Rate (Aerocapture)	500 W/cm^2
Peak Aerocapture Heat Rate (Convection)	450 W/cm^2
Peak Aerocapture Heat Rate (Radiation)	130 W/cm^2
Peak Heat Rate (Entry)	130 W/cm^2
Peak Entry Heat Rate (Convection)	130 W/cm^2
Peak Entry Heat Rate (Radiation)	20 W/cm^2
Total Heat Load (Aerocapture + Entry)	80 kJ/cm^2
Heat Load (Aerocapture)	55 kJ/cm^2
Heat Load (Entry)	25 kJ/cm^2
Peak Pressure	
Peak Pressure (Aerocapture)	45 kPa
Peak Pressure (Entry)	25 kPa
Peak Shear Force	
Peak Shear Force (Aerocapture)	700 Pa
Peak Shear Force (Entry)	300 Pa

Preliminary analyses of heatshield requirements were performed using the aerocapture and entry trajectories as driving boundary conditions.[1-2] Using Phenolic Impregnated Carbon Ablator (PICA), with a density of 0.28 g/cm^3, as the baseline material for the heatshield, these analyses showed that a margined thickness of 14 cm would be required to maintain a bondline temperature limit between the heatshield and the structure.[1] Further analyses showed that this thickness would result in a marked reduction in the delivered payload due to the mass of the heatshield. Thus, the EDL TDP sought to procure and develop material systems that can meet the heating requirements with at least a 25% reduction in mass and a goal of 50% reduction in the mass over PICA.

In early 2010 the EDL TDP solicited proposals for screening of rigid TPS for a mid L/D rigid aeroshell. Eight TPS materials were subsequently evaluated during the Round 1 Screening Phase, and three of those materials were recommended for a follow-on development phase. This paper focuses on the follow-on Round 1 Development Phase of rigid TPS materials, which took place in 2011. The three vendors and their dual-layer materials selected to provide rigid ablative TPS for Phase 1 Development are discussed in Table 2, and shown in Figure 3.

Table 2. Rigid TPS materials evaluated in by EDL TDP.

Material Vendor	Material System (Abbreviation)	Ablative Layer	Insulation Layer
Applied Research Associates (ARA)	PhenCarb 28 over PhenCarb 15 (PhenCarb 28/15)	P-28	P-15
Boeing	Boeing Phenolic Ablator-Functionally Graded (BPA-FG)	BPA-HD	BPA-LD
Lockheed Martin Space Systems	Graded MonA (MonA)	MonA-HD	MonA-LD

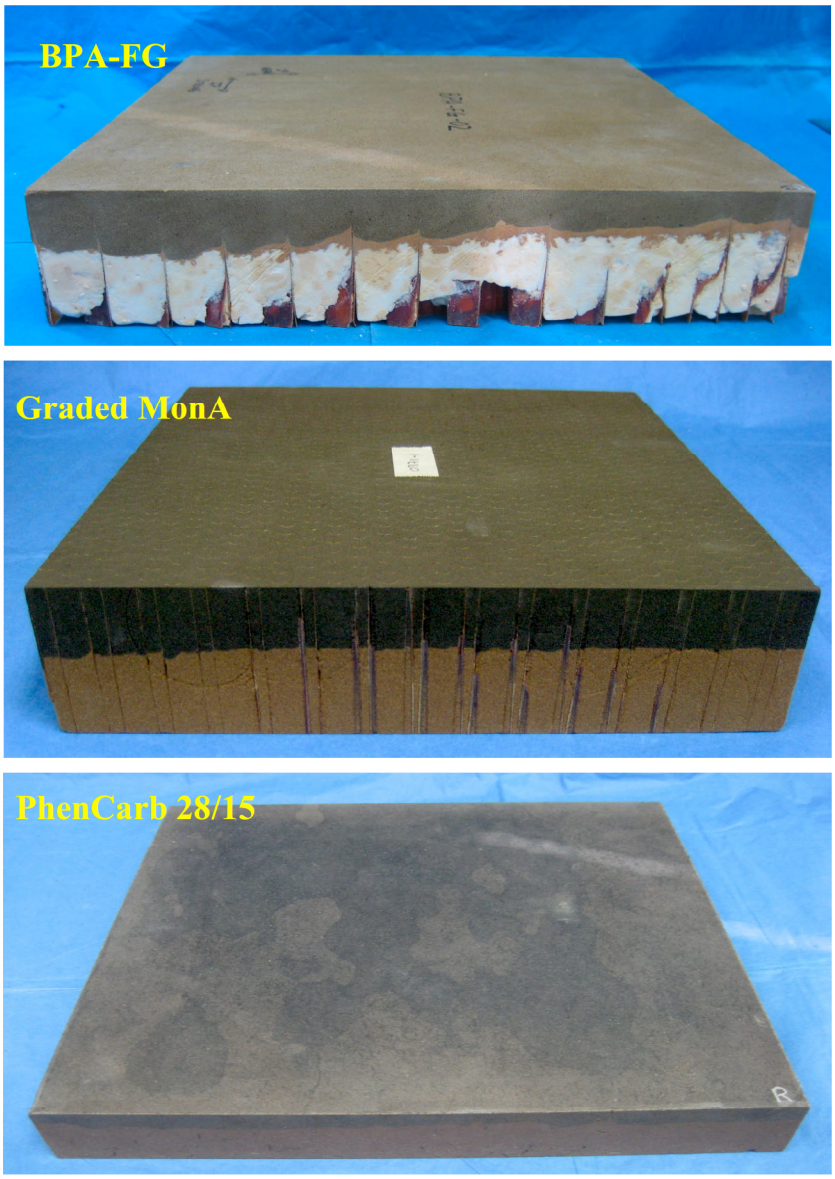

Figure 3. Dual layer TPS billets provided by vendors, approximately 30 cm on each side and 5 cm thick

ARA provided a dual layer material, PhenCarb 28 over PhenCarb 15. PhenCarb is a phenolic thermoplastic system that contains high proportions of cured phenolic polymer resin combined with reinforcing fibers, low density fillers, and honeycomb reinforcement. Boeing provided Boeing Phenolic Ablator-Functionally Graded (BPA-FG) test specimens, which is a medium-density phenolic syntactic foam with honeycomb reinforcement. The "dual-layer" test specimens consisted of an outer layer of BPA-Low Cure Temperature layer over a layer of lower density BPA. Lockheed Martin Space Systems provided Graded Monolithic Ablator (Graded MonA) test specimens. The MonA material consists of a PICA-like mixture packed into a honeycomb reinforcement, which is then cured. Like the other two systems, MonA has a higher density outer layer over a lower density insulative layer. The baseline material for comparison was PICA, manufactured by Fiber Materials, Inc. It was included in this test series since it is considered the current state-of-the-art. PICA material consists of a low density, fibrous carbon substrate infiltrated with phenolic resin. Residual PICA material from the manufacture of the Mars Science Laboratory heatshield was utilized to produce the test specimens.

Development testing of the three selected TPS materials included physical and structural properties evaluations as well as thermal response evaluation in an arcjet using a simulated air atmosphere. Additional arcjet testing in a

simulated Martian CO_2 atmosphere is to take place in late 2011 as this paper is being submitted. A summary of all testing is discussed in the following sections.

II. Physical Property Characterization

A. Property Characterization Overview

Characterization of the EDL candidate TPS materials consisted of a suite of material properties that were gathered to aid in thermal and ablation response model development as well as finite element modeling for each material system. Each of the three developmental material systems, Boeing's BPA-FG, Applied Research Associate's Phencarb 28/15, and Lockheed Martin's MonA, consists of two layers. All layers were characterized in order to facilitate high fidelity modeling. Properties that are key to thermal and ablation modeling are listed in Table 3 and include thermal transport properties such as thermal conductivity and thermal diffusivity, and physical properties such as density, composition, specific heat, emissivity and char yield. It is important to measure thermophysical properties as a function of temperature in order for physics-based response models to be constructed over a range of conditions.

In addition to basic thermal and physical properties of materials, several fundamental mechanical properties are needed for thermo-structural modeling; these properties include tensile modulus, tensile strain to failure, tensile strength and thermal expansion. During this effort, the tensile properties of candidate materials were measured in both in-plane and through-thickness orientations, and these results are summarized in Section III. Thermal expansion for each material was only measured in the in-plane orientation since this is the orientation that is constrained by attachment to entry vehicles. A complete list of the thermal and physical properties measured in this study is listed in Table 3. Since all three TPS vendors provided dual layer systems, a total of six unique materials were characterized. An exception to this is for BPA-LD, which proved too brittle and fragile in machining to obtain all of the specimens. All properties were measured on a single manufacturing lot for a given TPS.

Three of the most critical thermal properties for response modeling include bulk density, specific heat capacity and thermal conductivity.[3-5] The system and layer densities for EDL TDP materials are presented in Table 4 alongside state-of-the-art materials PICA and Avcoat. PICA was used for the heatshields of Stardust and MSL[**], while Avcoat is currently undergoing qualification testing for the Orion Multipurpose Crew Vehicle heatshield. The following sections give some results for the specific heat and conductivity. Given the export control restrictions for material properties of ablative TPS, the detailed results will not be presented here, but rather an overview of thermal conductivity determinations is provided with normalized data presented.

[**] MSL launched on 11/25/2011 and is planned to enter the Mars atmosphere on 8/5/2012

Table 3. Thermal and physical properties acquired for all three EDL TPS development material systems.

#	Property	Method	Notes/Conditions
1	Density (virgin)	Bulk density	-
2	Density (char)	Bulk density	Oven char
3	Char yield	TGA	RT to 1000 °C, N_2
4	Elemental Composition (virgin)	Combustion & ICP-OES	C,H,N,Si,Al,Ca,Mg,B,Na
5	Elemental Composition (char)	Combustion & ICP-OES	C,H,N,Si,Ca
6	Heat of Combustion (virgin)	Bomb calorimetry	-
7	Heat of Combustion (char)	Bomb calorimetry	-
8	Thermal Conductivity, TTT (virgin)	ASTM E1225	RT to 240 °C
9	Thermal Diffusivity, TTT (virgin)	Laser Flash	RT to 240 °C
10	Thermal Diffusivity* TTT (virgin)	*Step Heating	RT to 240 °C
11	Specific Heat (virgin)	DSC	RT to 240 °C
12	Specific heat (char)	DSC	RT to 400 °C
13	Thermal Expansion IP (virgin)	Dilatometry	RT to 240 °C
14	Emissivity (char)	Scanning radiometer	During arc jet testing
16	Tensile Strength (virgin)	Flatwise Tension	RT
17	Tensile Modulus (virgin)	Flatwise Tension	RT
18	Tensile Strain to Failure (virgin)	Flatwise Tension	RT

Table 4. TPS density comparison.

Material	Layer Density, g/cm^3	System Density, g/cm^3
BPA-LD	0.16	0.31
BPA-HD	0.46	
MonA-LD	0.25	0.28
MonA-HD	0.31	
Phencarb-15	0.26	0.38
Phencarb-28	0.50	
PICA	0.27	0.27
Avcoat	0.54	0.54

B. Thermal Conductivity Measurement Background

Thermal conductivity is a crucial property for TPS material thermal response modeling and typically has a large uncertainty which contributes to high margins and TPS mass fraction.[6-8] The uncertainty comes from two sources: 1) the variability typically observed in TPS materials in terms of density, composition, microstructure and therefore properties, and 2) the uncertainty in the measurement itself.

Material variability is typically greatest from lot to lot, but can be reduced over time through process refinement thereby leading to a narrower range of properties. This was observed over the course of PICA manufacture for the Orion and Mars Science Laboratory (MSL) programs wherein process refinements implemented to reduce material variability also reduced the range of PICA properties measured during lot acceptance testing.[9,10]

Thermal conductivity measurements of TPS materials prove to be difficult as the variety of available techniques each have challenges. Table 5 shows the most commonly used techniques for determining thermal conductivity of TPS materials. All methods in Table 5 strive to achieve one-dimensional heat flow, either via guarded heating and long equilibration times (steady state techniques) or rapid heat diffusion through a very thin specimen (transient techniques).

Table 5. Thermal conductivity and thermal diffusivity measurement techniques employed for TPS materials.

Method	Type	Specimen Size, cm	Notes
Guarded Hot Plate (ASTM C 177)	Conductivity, Steady State	Diameter: > 18 Thickness: 0.5 – 2	Direct measurement; preferred for most TPS materials
Comparative Longitudinal Heat Flow (ASTM E 1225)	Conductivity, Steady State	Diameter: 2 – 5 Thickness: 0.5 – 5	Uses references calibrated by GHP; small sample size may not be representative of bulk.
Laser Flash (ASTM E 1461)	Diffusivity, Transient	Diameter: 1 – 2.5 Thickness: 0.5 – 3	Very small sample likely not representative of bulk; separate Cp measurement required for λ
Step Heating (ASTM E 1461)	Diffusivity, Transient	Diameter: 5 Thickness: 1 – 3	Small sample may not be representative of bulk; separate Cp measurement required for λ

The generally preferred method for TPS materials, and the most direct measurement of thermal conductivity, is via the guarded hot plate (ASTM C 177). The EDL TDP materials are highly porous and have conductivities that are well within the accuracy range for the guarded hot plate. This technique utilizes large specimens, typically greater than 18 cm in diameter and 1 to 3 cm thick. The relatively large volume of material is beneficial in terms of providing a representative sampling of a given manufacturing lot, but often exceeds the amount of material available, especially during early development activities such as the EDL TDP. As a steady-state method, data collection is very time consuming, typically requiring a week's time to obtain conductivity over a range of temperatures.

Comparative longitudinal heat flow (ASTM E 1225) is also a steady state method but requires less material with specimens typically 2 to 5 cm in diameter and 1 to 2 cm thick. Although the smaller sample size is more convenient, it can also be less representative of TPS materials, especially those that have unit cells (such as honeycomb) that are similar or larger in size compared to the specimen. This method relies on the use of standard materials, and has an ideal range of measurement that is at or above the conductivity of most NASA TPS materials, including those discussed here.

A convenient and frequently used approach for obtaining thermal conductivity of TPS materials is by measuring thermal diffusivity (α), specific heat (Cp) and density (ρ), and calculating conductivity (k) from equation 1.

$$k = \alpha . \bullet Cp \bullet \rho \tag{1}$$

However, this approach has some significant shortcomings. The thermal diffusivity can be determined by laser flash (ASTM 1461) or step heating.[11] Diffusivity specimen sizes are typically 1 to 5 cm in diameter and only 0.25 cm thick. This small volume does not usually capture a representative quantity of material with respect to unit cell size or inherent material variability. Furthermore, these techniques are not ideal for porous materials such as those in the EDL TDP.

Specific heat is typically determined by differential scanning calorimetry (DSC). The key challenge for virgin ablator specific heat determination by DSC stems from the fact that the resin systems present in ablative TPS undergo curing and other secondary reactions over the temperature range of interest. Thus pre-conditioning of the sample to the maximum temperature of interest is required to obtain reasonable specific heat data, and the exact conditions used will influence the DSC results. Oftentimes, post-cure reactions are still observed by DSC, and the curves are smoothed to remove the reaction, further reducing the accuracy of the specific heat determination. Finally, since three separate measurements are required to obtain thermal conductivity this way, the propagation of error can be appreciable.

C. Thermal Conductivity Determinations for EDL TDP

For this project, thermal conductivity was determined on each of the TPS material layers in four separate laboratories using three different techniques according to Table 6. The detailed data will not be shown here due to export control restrictions; however, a relative comparison of techniques and materials is provided. All of the thermal property specimens were removed from the same area of a given piece of TPS material to maximize homogeneity of the samples for inter-lab comparisons. Material variability between lots was not captured in this effort.

Table 6. Thermal conductivity/diffusivity test matrix for EDL TDP materials.

Property	Method	Laboratory	Notes/Conditions
Density (virgin)	Bulk density	All	on each specimen
Thermal Conductivity, TTT (virgin)	ASTM E1225	SoRI	RT to ca. 240 °C
Thermal Diffusivity, TTT (virgin)	Laser Flash	ARC, JSC	RT to ca. 240 °C
Thermal Diffusivity* TTT (virgin)	*Step Heating	TPRL	RT to ca. 240 °C
Specific Heat (virgin)	DSC	ARC, JSC, TPRL	RT to ca. 240 °C

The specific heat measurements made for determining conductivity from thermal diffusivity had good repeatability within each of the three labs (ARC, JSC, TPRL) that measured it, but inter-lab variability was a bit higher. The specific heat, averaged for each lab's results and normalized to provide relative comparison, for two of the materials measured is shown in Figure 4.

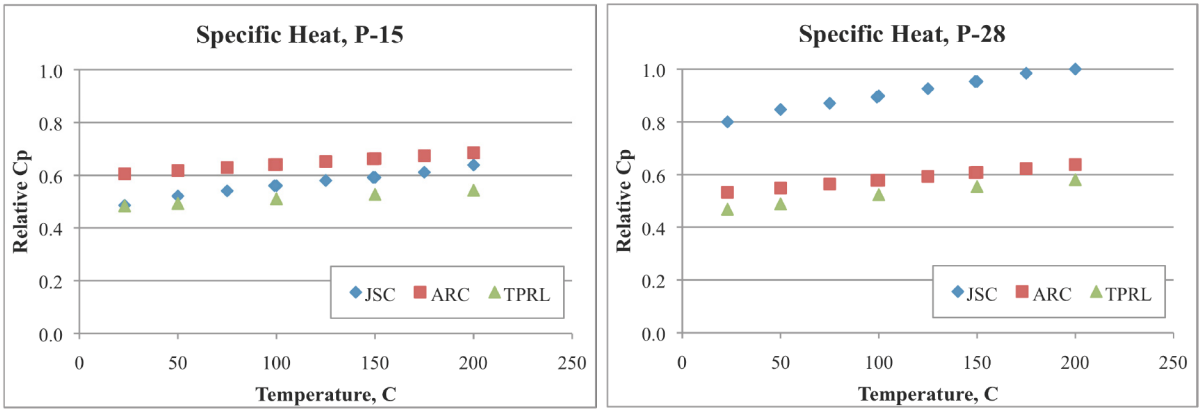

(a) (b)

Figure 4. Specific heat plots showing: a) good agreement between labs (observed for most materials), and b) moderate variability between labs (observed for two materials).

ARC and Johnson Space Center (JSC) both showed good repeatability for their laser flash diffusivity measurements; only one measurement per material was obtained using TPRL's step heating. The consistency between labs was lower for thermal diffusivity (Figure 5) than it was for specific heat, which is likely due to both material variability (diffusivity is sensitive to microstructure whereas specific heat is not) and measurement error.

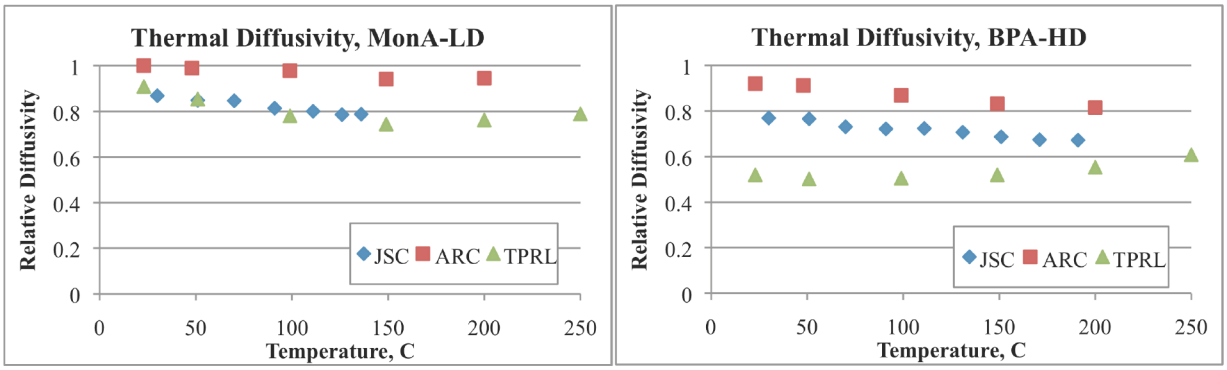

(a) (b)

Figure 5. Thermal diffusivity plots showing: a) best agreement observed between labs, and b) worst inter-lab agreement observed

The range of thermal conductivities resulting from each lab's measurements is depicted for two materials in Figure 6. With the exception of SoRI's comparative conductivity test, the values were determined from thermal

diffusivity, specific heat and density as shown in Equation 1. In most cases the SoRI-determined conductivity was the highest while the TPRL determinations were the lowest. The consistency of results between labs was best for MonA-LD where SoRI's values were about 150% of those from TPRL. On the other hand, SoRI's results for BPA-HD were about 220% of those from TPRL. Each material's average conductivity from all labs (Figure 7) tended to be close to the laser flash values obtained by ARC and JSC.

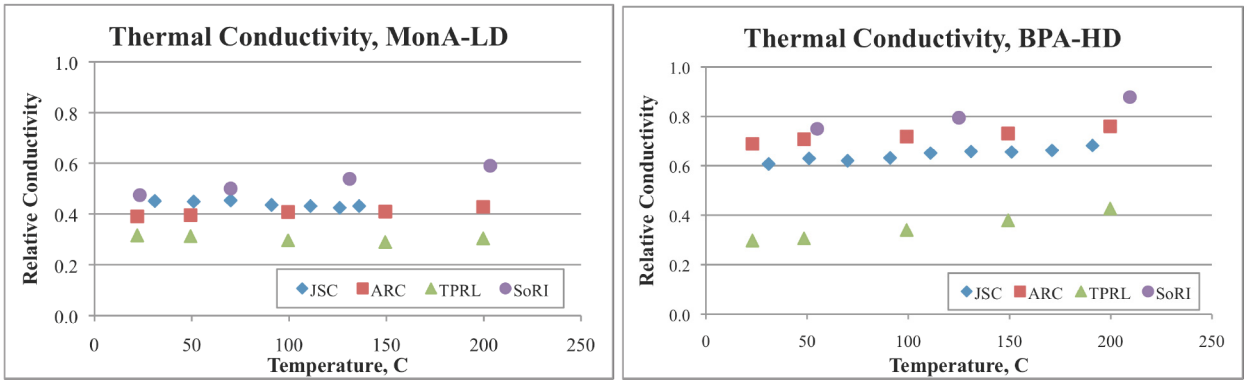

Figure 6. Thermal conductivity plots showing: a) best agreement observed between labs, and b) worst inter-lab agreement observed.

The thermal conductivity (average of all lab measurements) for each rigid EDL TDP material is shown in Figure 7 along with that of state-of-the-art TPS materials Avcoat and PICA for comparison purposes (results are normalized relative to PICA). All EDL TDP materials had thermal conductivities much lower than PICA and close to that of Avcoat. Since the TDP materials are lower in density than Avcoat (see Table 4), they all appear to have conductivity/density performance that is enhanced relative to the state-of-the-art TPS materials. While density and thermal conductivity are critical properties for TPS performance, they must be considered alongside the ablation and structural performance as well, which are discussed in the following sections.

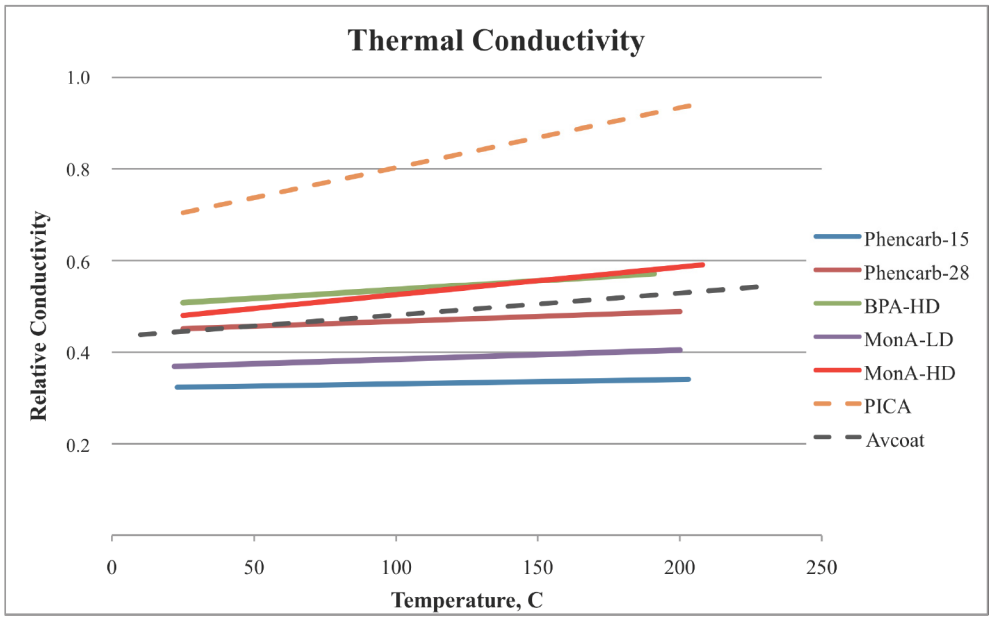

Figure 7. Relative thermal conductivity for the EDL TDP materials compared to PICA and Avcoat.

III. Structural Characterization

The purpose of the structural characterization testing was to determine the strain to failure, bending stiffness, curvature limit, and failure modes of the ablator materials. A combination of flatwise tensile (FWT) tests and three point flexure tests were used. FWT tests were conducted in both the through-the-thickness (TTT) and in-plane (IP) orientations.

A. Flexure Testing

Flexure tests used built-up specimens consisting of an ablator block directly bonded to an aluminum substrate with the 30.5 cm long by 7.6 cm wide ablator blocks, cut from billets supplied by the vendors, bonded onto the aluminum substrate using RTV-560. Machining and bonding of the ablator blocks, along with specimens for the other tests in Sections II and III, was performed by NASA Langley.

A concern of dual layer ablators was that the interface between layers would be weak. For this reason the aluminum substrate was designed with stress relief cuts and varying thickness to reduce the chance of failure at the ends of the ablator block and increase the shear and tension stresses in the middle of the ablator block, as shown in Figure 8. The stress relief cut was 3.18 cm in length, extended 2.54 cm under the ablator, and ran at a depth of 0.37 cm under the surface of the substrate. A 15.2 cm section of the substrate was reduced from 1.27 cm to 0.95 cm in thickness, centered on the substrate mid-span. Specimens were tested in a three point flexure apparatus installed in a hydraulic load machine. Span between the outer load points was 35.6 cm. Specimens were statically loaded to failure under displacement control at a rate of 0.064 centimeters per minute.

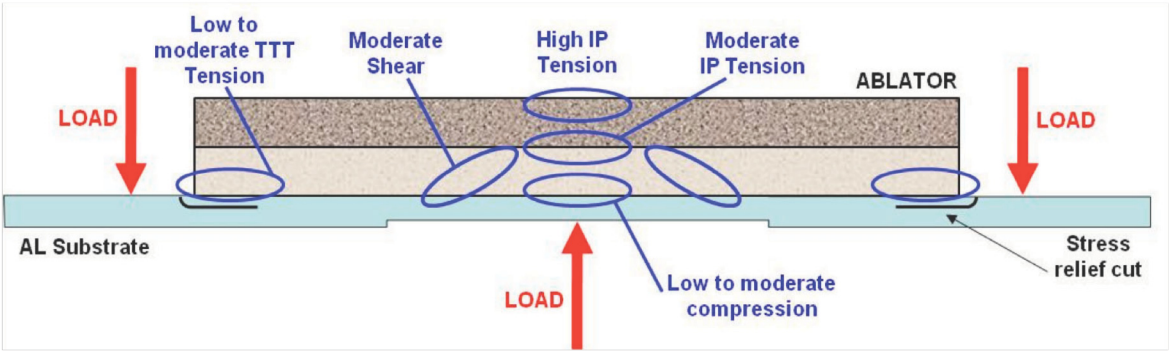

Figure 8. Flexure test specimen.

Billet inspection and fabrication of specimens revealed several defects in the ablators. All of the dual layer specimens exhibited considerable variability with respect to the HD/LD interface depth (see Figure 3). Graded MonA and PhenCarb 28/15 specimens had a 1.3 cm variation in interface location and BPA-FG specimens had as much as a 2.5 cm variation. During inspection of the BPA-FG billets it was noticed that several sections of the lower density material had fallen out around the edge of the billet and that adhesion between the lower density material and the honeycomb ribbon was poor. This was further substantiated during specimen fabrication, when thin layers of the lower density BPA layer fell apart, as shown in Figure 9. Inspection of Graded MonA billets revealed linear surface indications running along the ribbon to filler interface on the billet outer surface. In addition, light was visible through the interface of 0.63 cm thick high density MonA layers. PhenCarb 28/15 specimens had numerous voids, which appeared to be primarily in regions where adjacent flex core ribbons formed an irregular or long and narrow gap. Although specimen fabrication revealed flaws in the three ablators, it was also a positive test of the high density to low density ablator interface for each ablator. During fabrication numerous cutting operations were performed on the billets in different directions without any indication of separation at the high to low density interface, which would appear to be a positive indicator that these interfaces have adequate room temperature strength. The EDL TDP was unable to obtain a sufficient amount of PICA to perform flexure testing, and thus comparisons will not be made for flexural properties. Previous PICA measurements made by the Orion TPS Advanced Development Project used a flex configuration that was too dissimilar to allow comparisons.

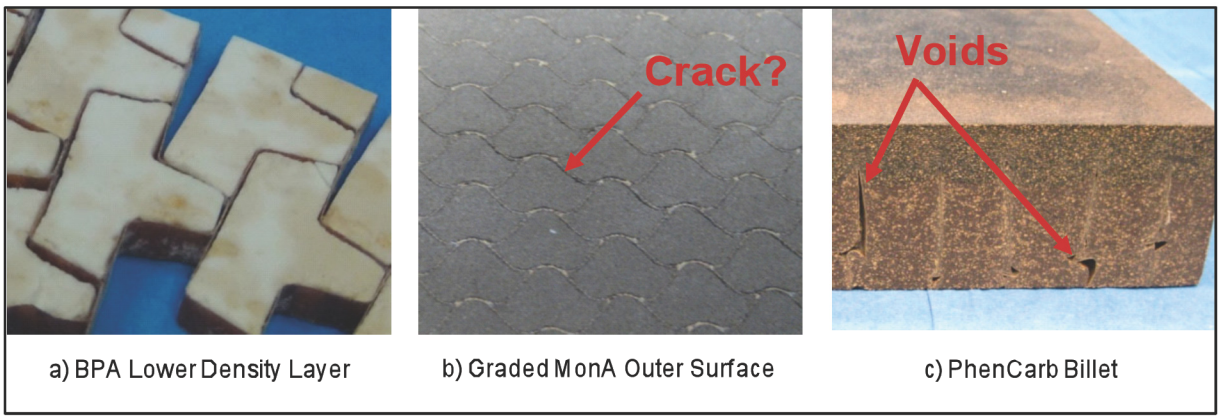

Figure 9. Pictures from inspection and fabrication.

Three specimens of each ablator type were tested in three point flexure. Results for the tests are summarized in Table 7. Failure Radius of Curvature (ROC) represents the substrate curvature at which the ablator fractured. The P/K entry represents the slope of the load (P) vs. curvature (K) graph and is a measure of the bending stiffness of the specimen. In addition to the nine ablator specimens, two bare substrates were tested for comparison. BPA-FG specimens failed at a relatively large radius of curvature and had a large bending stiffness. All BPA-FG failures occurred at the ablator ends with visible cracking in the lower density BPA layer. Figure 10 shows a typical failure, where the visible disbond occurred after fracture of the BPA layer. When Graded MonA specimens were tested in flexure, through-the-thickness cracks gradually opened up without any cracking sounds or noticeable jump in the instrumentation. In addition, the bending stiffness of MonA specimens was equivalent to that of the bare substrates, which leads to the conclusion that the linear indications observed during billet inspection were cracks through the thickness. A typical Graded MonA specimen under load is shown in Figure 11. Despite efforts to ensure good bonds, two of the three PhenCarb 28/15 specimens had bad bonds that failed immediately upon loading the specimen. It is not clear whether the bad bond was due to the bonding technique or the nature of the material being bonded. The remaining PhenCarb 28/15 specimen was considerably more compliant than BPA-FG. The specimen had a substantially lower bending stiffness and fractured at a relatively tight radius of curvature. Fracture was at the ablator end near the bondline, as shown in Figure 12.

Table 7. Flexure test results.

Ablator Type	Ablator Thickness (cm)	Failure ROC (m)	Failure Location	P / K (N-m)
BPA 01	6.22	18	End	21,128
BPA 02	6.22	17	End	21,919
BPA 03	6.22	20	End	19,094
MonA 01	5.64	N/A	N/A	4,542
MonA 02	5.64	N/A	N/A	4,395
MonA 03	5.64	N/A	N/A	4,180
PhenCarb 01	4.52	Bad Bond	Bond	N/A
PhenCarb 02	4.52	5.4	End	10,123
PhenCarb 03	4.52	Bad Bond	Bond	N/A
Bare Plate 15	N/A	N/A	N/A	4,365
Bare Plate 16	N/A	N/A	N/A	4,330

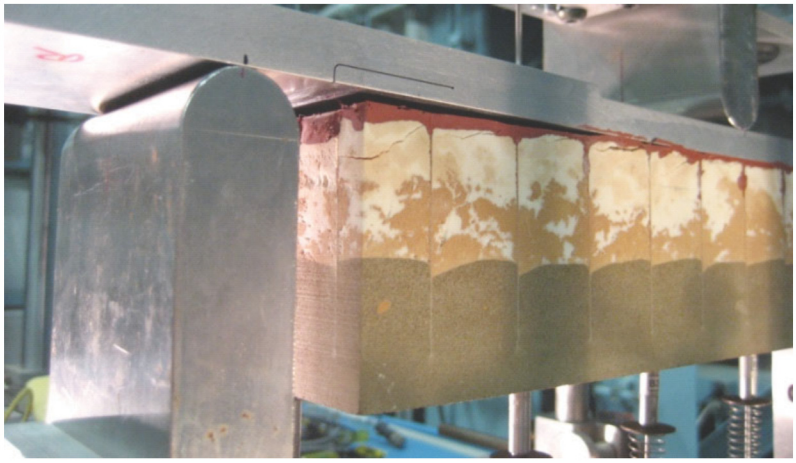

Figure 10. BPA-FG specimen during flexure test.

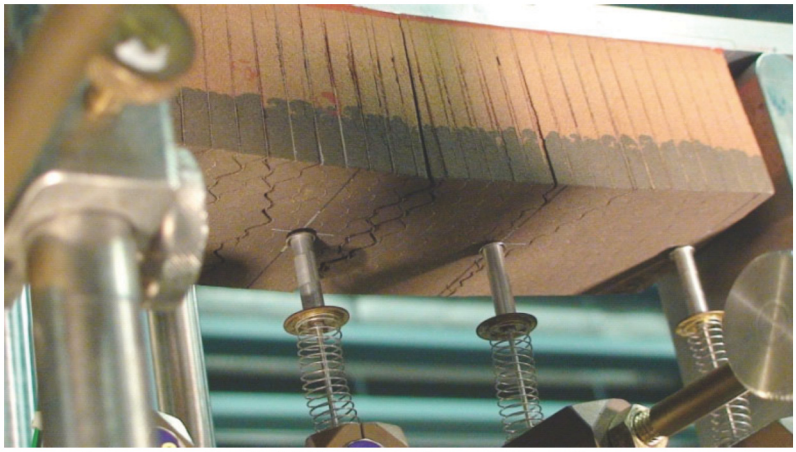

Figure 11. Graded MonA specimen during flexure test.

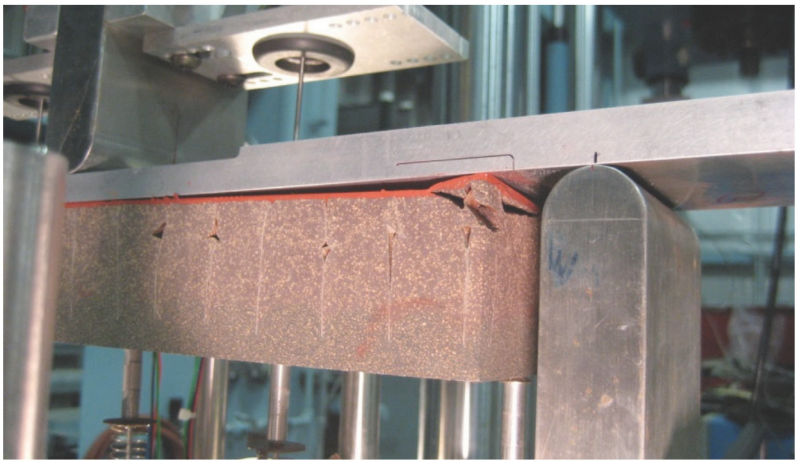

Figure 12. PhenCarb 28/15 specimen during flexure test.

B. Flatwise Tensile Testing

Tests in the TTT orientation were conducted on the entire ablator thickness and had a 7.6 cm by 7.6 cm cross section. Tests in the IP orientation were performed on the individual low and high density layers of each ablator,

and were conducted in the weak orientation with respect to the honeycomb core. High density layer specimens were 1.3 cm thick by 7.6 cm wide and had a length of 7.6 cm. Low density layer specimens were 2.5 cm thick by 7.6 cm wide and had a length of 7.6 cm. All flatwise tensile specimens were bonded to aluminum blocks with epoxy and tested in a hydraulically actuated test stand. Strain measurements were made using clip-on extensometers. Three tests were run per specimen and orientation type.

Flatwise tension test (FWT) are summarized in Table 8. A key finding was that none of the layers of the various ablator materials were able to achieve the EDL TDP Key Performance Parameter of 1% strain-to-failure when tested in in-plane tension. Instead of significantly improving on this metric with respect to PICA, all materials except PhenCarb-28, and this high density layer of PhenCarb only achieved 0.56% strain before failure. MonA was excluded from the strain comparison due to the presence of through-thickness cracks. A positive result of the through-the-thickness tension testing was that there were no failures noticed at the high to low density interface, indicating that the interface layer is not the weak link. In-plane testing of BPA-HD indicated that it had a high modulus and strength, but a relatively low strain-to-failure. The BPA-LD layer had very low strength, presumably due to the observed poor filler-to-honeycomb ribbon adhesion. The PhenCarb 28 layer was more compliant than BPA and failed at a higher strain-to-failure. The PhenCarb 15 layer had a considerably lower modulus than PhenCarb 28, but failed at a lower strain. In-plane testing of both MonA-HD and MonA-LD confirmed the presence of through-thickness cracks (disbonded at the filler to honeycomb ribbon interface), since strength properties were very low.

Table 8. Summary of flatwise tensile test results, average of 3 specimens per material/orientaiton.

Material	Orientation		Fracture Stress (kPa)	Modulus (MPa)	Strain at Fracture (%)	Failure location
BPA (full thickness)	TTT	**average**	**1,000**	**728**	**0.20**	low-density layer
		Std Dev	4.7	16.1	0.03	
BPA-HD	In-Plane	**average**	**4,516**	**1,389**	**0.33**	filler
		Std Dev	122.2	6.5	0.06	
BPA-LD	In-Plane	**average**	**64**	**67**	**0.13**	filler/honeycomb core debond
		Std Dev	5.4	5.8	0.03	
MonA (full thickness)	TTT	**average**	**2,446**	**506**	**0.57**	two in HD layer, one in LD layer
		Std Dev	82.6	7.2	0.15	
MonA-HD	In-Plane	**average**	**110**	**113**	**0.39**	filler/honeycomb core debond
		Std Dev	8.9	9.5	0.24	
MonA-LD	In-Plane	**average**	**121**	**94**	**0.27**	filler/honeycomb core debond
		Std Dev	5.4	3.9	0.13	
PhanCarb 28/15 (full thickness)	TTT	**average**	**952**	**336**	**0.32**	low-density filler
		Std Dev	5.8	1.0	0.02	
PhenCarb-28	In-Plane	**average**	**3,477**	**666**	**0.56**	filler
		Std Dev	43.6	6.1	0.03	
PhenCarb-15	In-Plane	**average**	**550**	**177**	**0.34**	filler + filler/honeycomb debond
		Std Dev	17.4	0.9	0.09	
PICA (Reference 10)	TTT	**average**	**325**	**49**	**0.75**	in ablator
	In-Plane	**average**	**1,245**	**393**	**0.35**	in ablator

IV. Thermal Response (Arcjet) Characterization

A. Arcjet Background

Thermal response arc-jet testing is used to evaluate TPS at a wide range of heat fluxes, pressures, and enthalpies representative of environments anticipated during various reentry trajectories and different locations on a prospective heat shield. There are typically two objectives to these tests. The first objective is to evaluate the in-depth thermal response of each TPS material using multiple thermocouples spaced throughout the sample from surface to backface. The second objective is to obtain recession data and evaluate char formation and identify unexpected failure modes.

All testing of this kind is typically performed in a stagnation regime, i.e., with the front surface of the test model perpendicular to the flow. The final outcome of the testing will be an extensive database of surface temperatures, in-depth temperatures, and recession data at well-defined arc-jet conditions that will aid in defining ablation thermal response models for each TPS material under consideration. Thermal response model (stagnation) tests in air were performed in the Atmospheric Reentry Materials and Structures Evaluation Facility (ARMSEF) at NASA Johnson Space Center during the period of September 19 – September 21, 2011. Additional tests in a carbon dioxide atmosphere are on-going and are not included in this paper. The test series was intended to provide data for thermal response model development and had the following test objectives:

1. Obtain mass loss and recession data for material concepts at relevant Mars aerocapture heating conditions in both air and Martian plasma environments
2. Obtain surface and in-depth thermal response of material concepts at relevant Mars aerocapture heating conditions in both air and Martian plasma environments (note Martian plasma testing pending at time of print)

Tests were conducted in the 10 MW ARMSEF Test Position 2 (TP2), with a dual diameter constricted arc column attached to a 15° half-angle conical nozzle. A tungsten button cathode was used as the upstream electrode of the arc heater; and a conical copper anode was used as the downstream electrode.[12] The arc heater contains a variable number of individually water-cooled and electrically insulated constrictor segments assembled in modular packs, 18-20 segments each.[12] The electrically heated test gas was expanded into the nozzle and ejected into the test chamber. As the heated gas passes the surface of the test article, the required surface heat fluxes were generated. For this test series a 12.7-cm (5-inch) diameter nozzle exit was used, and each test article was situated 20 cm from the nozzle exit plane. The air test gas, 23 percent O_2 and 77 percent N_2 by mass, is injected at various places along the column's length, and nitrogen is always injected in the vicinity of the tungsten cathode to reduce cathode oxidation.[12] Real time video coverage of the test article surface was provided by a video camera mounted outside the test chamber, and a second video camera monitored the interior of the vacuum chamber.

Table 9 lists the targeted cold wall heat flux test conditions of interest, as referenced to a 10.2-cm diameter flat-face model/calorimeter. Phenolic Impregnated Carbon Ablator, considered the current state-of-the-art and manufactured by Fiber Materials, Inc. (FMI), was also included in this test series. Test conditions were determined from calibration runs prior to testing the development material test articles. Several calibration runs were completed in separate runs to determine the facility settings necessary to meet the test condition requirements, and to verify repeatability of the test condition.

Table 9. Stagnation arcjet test conditions.

Condition ID	Target Conditions				Cal Index	Mass Flow	Current	Slug Cal Reading			
	Heat Flux		Pressure					Heat Flux		Pressure	
	W/cm^2	BTU/ft^2-sec	atm	psf		lb/sec	amps	W/cm^2	% err	atm	% err
TP-044 Rigid A	150	132.1	0.150	317.5	2-3816-1D	0.45	620	154.9	3.2%	0.147	-1.7%
TP-044 Rigid A	150	132.1	0.150	317.5	2-3816-1G	0.45	620	153.5	2.3%	0.147	-1.7%
TP-044 Rigid B	450	396.2	0.350	740.7	2-3817-1B	0.93	1550	465.0	3.3%	0.354	1.3%
TP-044 Rigid B	450	396.2	0.350	740.7	2-3817-1C	0.93	1550	479.0	6.5%	0.352	0.7%

All test specimens were machined and instrumented by NASA Ames from vendor-supplied billets. Ablator test specimens consisted of 10.2-cm diameter flat-face pucks with a thickness of 4.57-cm, as shown in Figure 13, and included one type-R and three type-K thermocouples. Samples were bonded to LI-2200 holders fitted with a threaded adapter that interfaced to the JSC arcjets.

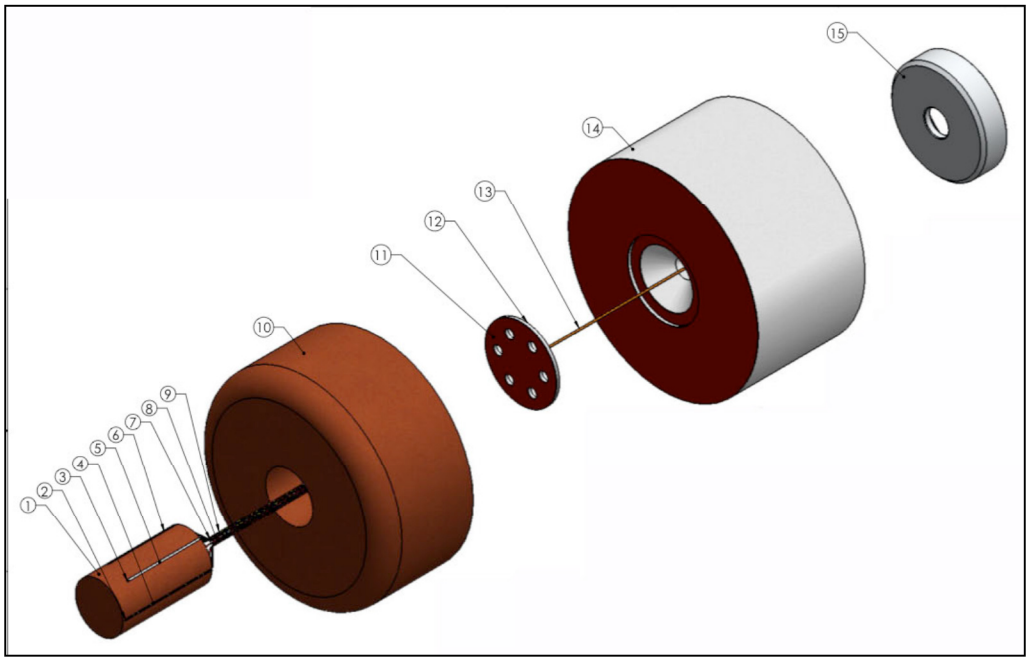

Figure 13. Stagnation arcjet model configuration.

B. Arcjet Results

Table 10 summarizes the arcjet test results for the three dual-layer vendor materials: Boeing's BPA, ARA's Phencarb 28/15, and Lockheed's MonA tested in simulated air.

Sample ID	Material	Target Heat Flux (W/cm^2)	Stagnation Pressure (kPa)	Test Time (sec)	Mass Loss (g)	Stagnation Point Recession (mm)	Average Recession Rate (mm/s)	Char Depth (mm)	Peak Surface Temp. (°C)	Peak Backface Temp. (°C)	Areal Weight (g/cm^2)
BPA-01	BPA-FG	150	15	90	33.1	4.3	0.05	8.4	1777	89	1.97
BPA-02	BPA-FG	150	15	90	33.5	4.8	0.05	9.0	1741	90	1.97
BPA-03	BPA-FG	450	35	60	53.6	11.6	0.19	4.6	2261	77	1.92
BPA-04	BPA-FG	450	35	60	53.8	10.8	0.18	4.7	2201	79	1.97
ARA-08	PhenCarb 28/15	150	15	90	25.0	4.0	0.04	8.0	1796	78	1.46
ARA-09	PhenCarb 28/15	150	15	90	25.0	4.1	0.05	8.2	1760	71	1.46
ARA-10	PhenCarb 28/15	450	35	60	50.2	9.8	0.16	3.8	2276	64	1.46
ARA-11	PhenCarb 28/15	450	35	60	48.9	9.8	0.16	4.3	2224	64	1.51
MONA-15	Graded MonA	150	15	90	32.7	12.5	0.14	6.9	1752	65	1.23
MONA-16	Graded MonA	150	15	90	33.1	12.5	0.14	6.9	1796	67	1.23
MONA-17	Graded MonA	450	35	60	55.1	22.7	0.38	2.5	2230	61	1.23
MONA-18	Graded MonA	450	35	30	29.0	11.9	0.40	3.1	2201	44	1.23
FMI-22	MSL PICA	150	15	90	27.1	9.5	0.11	5.4	1812	180	1.37
FMI-23	MSL PICA	450	35	60	33.9	12.3	0.20	5.1	2327	175	1.37

Table 10. Summary of post-test rigid ablators arcjet testing.

1. PICA Results

Since PICA is considered the state of the art, its performance provides a reference for all other material results. One PICA test article was tested at each test condition. Table 10 shows the test results for each PICA test article compared to BPA, PhenCarb and MonA. The PICA test articles showed uniform ablation and a smooth post-test surface. Essentially the same peak backface temperature was reached, even though the lower heating condition was half the total heat load of the high heating condition. This result demonstrates the increased ablative efficiency at higher heating conditions. Test article FMI-23, tested at the higher heat flux, had a stagnation point recession 30%

higher than test article FMI-22, and a similar char depth result to test article FMI-22. Most in-depth thermocouples burned out during the test exposure as the material receded past the thermocouple depth.

2. BPA-FG Results

Two BPA-FG test articles were tested at each heating condition, and the results were repeatable for each test condition, as shown in Figure 14. At the low heating condition the surface had a glass melt layer, and at the high heating condition, a uniform char layer formed. BPA-FG test articles at the higher heating condition experienced recession about 2.5 times higher than at the lower heating condition. At the lower heating condition, the resultant recession was about half that of PICA at the same heating condition. At the higher heating condition, however, the BPA-FG recession was similar to that of PICA. BPA-FG had a peak backface temperature about 90 °C lower than that of PICA at the lower heating condition, and like PICA, had a slightly lower peak backface temperature for the higher heating condition when compared to the lower heating condition. At the lower heating condition, BPA-FG char depth was about double that of the higher heating condition, and was the deepest char layer of all materials tested at this condition. The delineation of the two layers can clearly be seen in the cross-section pictures, and shows a relatively thick outer ablative (high density) layer. Although all dual layer ablator systems had pronounced interface waviness between the two layers, it was most prominent in BPA-FG.

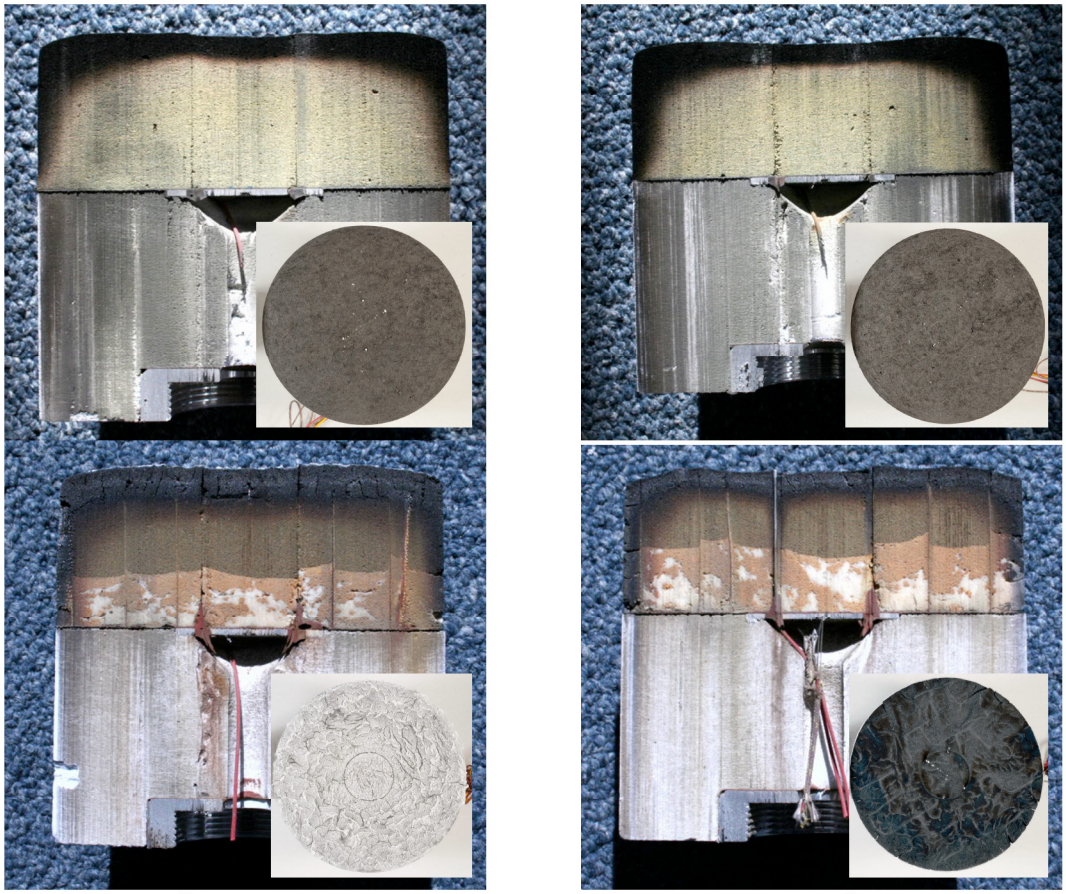

150 W/cm^2 (90 seconds) **450W/cm^2 (60 seconds)**

Figure 14. Photos of MSL PICA (top) and BPA (bottom) after arcjet testing at 150 and 450 W/cm^2.

3. PhenCarb 28/15 Results

Two PhenCarb 28/15 dual layer test articles were tested at each condition, and the results were repeatable. As shown in Figure 15, similar to the BPA-FG results, a melt layer formed at the lower heating condition, and a char layer formed at the higher heating condition. For the lower heating condition, there was more recession in the center of the model than at the edges. At the higher heating condition, PhenCarb 28/15 test articles had a recession about

2.5 times higher than at the lower heating condition. At the lower heating condition, PhenCarb 28/15 had a recession about 2.4 times less than PICA at the same condition. At the higher heating condition, PhenCarb 28/15 had a recession of only about 25 percent less than that of PICA at the same condition. PhenCarb 28/15 had a peak backface temperature about 100 °C less than PICA at the lower heating condition, and like the other materials, had a lower peak backface temperature at the higher heating condition.

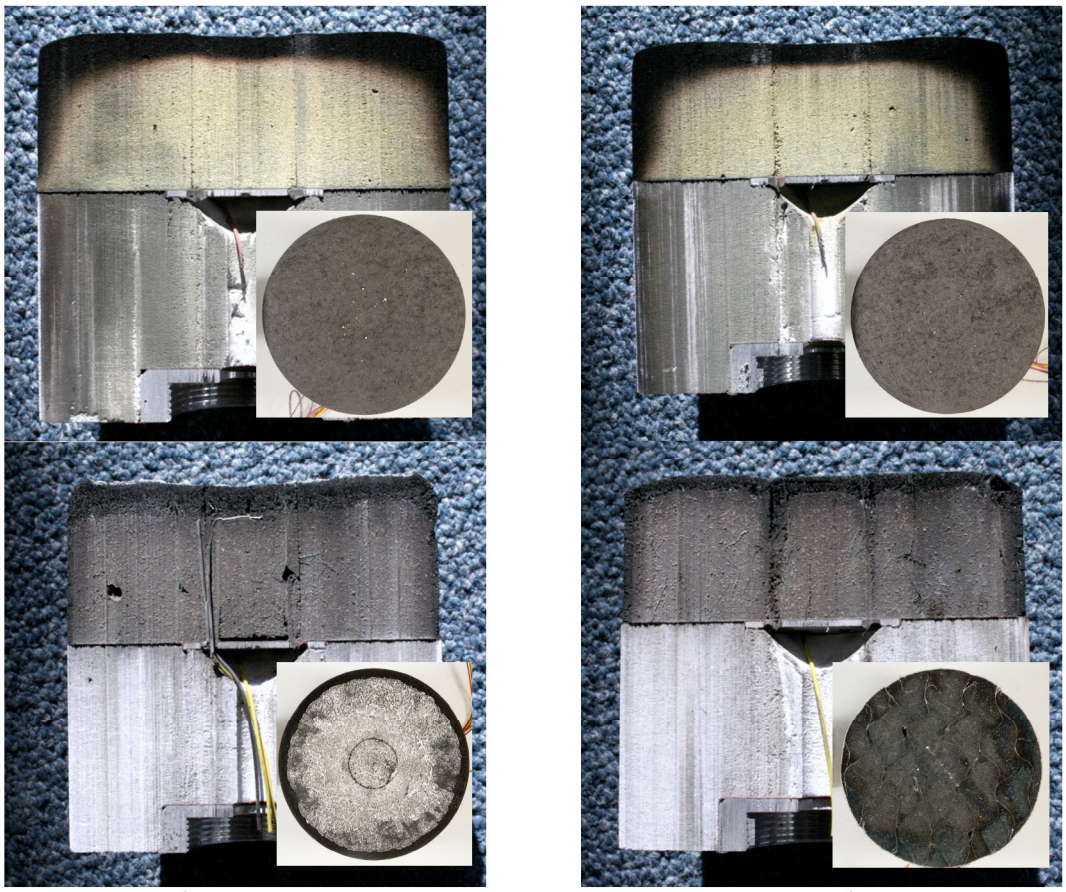

150 W/cm^2 (90 seconds) **450W/cm^2 (60 seconds)**

Figure 15. Photos of PICA (top) & PhenCarb 28/15 (bottom) after arcjet testing at 150 & 450 W/cm^2.

4. Graded MonA Results

Two Graded MonA test articles (Figure 16) were tested at each heating condition; however, the test duration for the second test article at the higher heating condition (MonA-18) was reduced by half after a large amount of recession was observed for MonA-17. Graded MonA experienced the highest recession, but maintained the lowest peak backface temperatures of all materials in the test matrix. Total recession and mass loss for MonA-18 were about half that of MonA-17, demonstrating performance repeatability. At the lower heating condition, Graded MonA recessed about 30% more than PICA at the same condition, and had a fairly uniform post-test surface. Comparing MonA-17 with FMI-23, Graded MonA recessed almost double that of PICA at this higher heating condition. At this high heating condition, Graded MonA had the thinnest char layer of all materials tested.

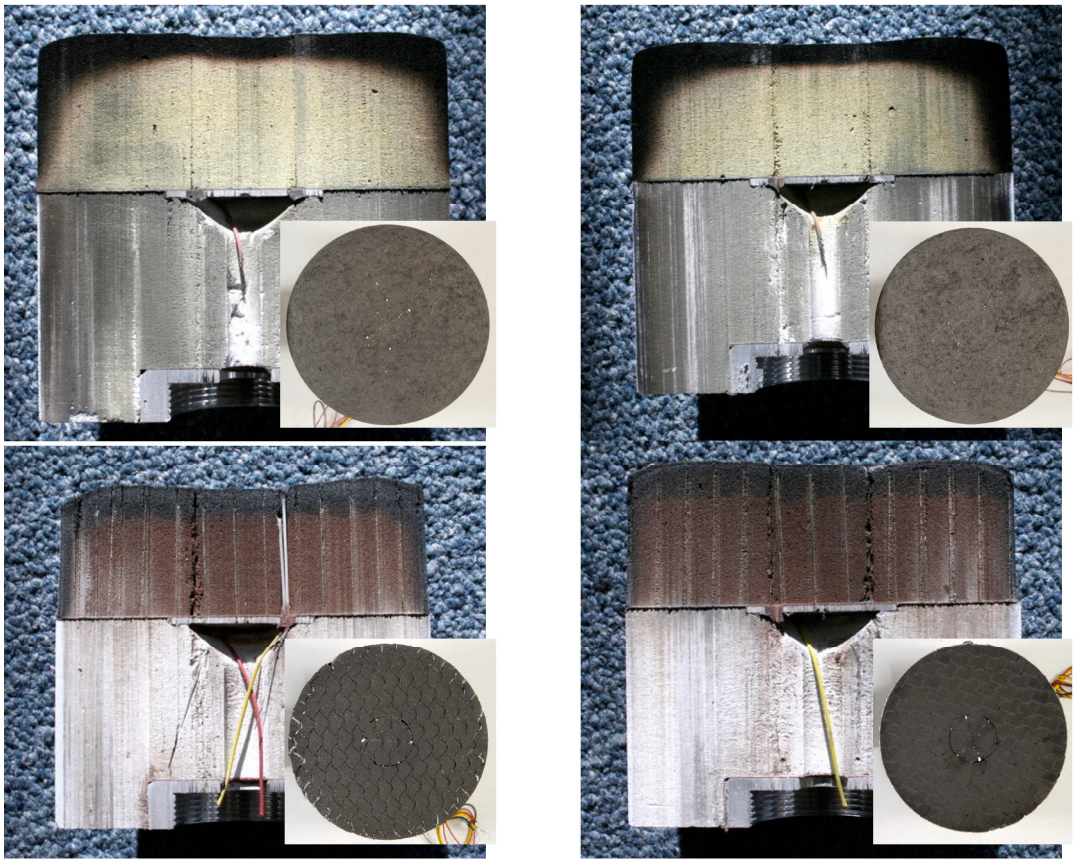

150 W/cm^2 (90 seconds) 450W/cm^2 (60 seconds)

Figure 16. Photos of MSL PICA (top) and MonA (bottom) after arcjet testing at 150 and 450 W/cm^2.

C. Material Performance Comparisons

Figures 17 and 18 show the recession rate and peak backface temperature results for the test articles at the lower heating condition, respectively. The plots show a general trend of decreasing recession rate with increasing outer layer char density, as would be expected, and, excluding PICA, a slight peak backface temperature increase with increasing aerial density. It should be noted, however, that the initial temperatures for BPA-FG test articles were consistently about 10°C higher than the other test articles. Some variation in initial temperatures was seen across the materials and was likely due to material porosity and water pick-up prior to the chamber reaching vacuum levels. The Graded MonA shows excellent insulative properties for a low areal weight, although it has the highest recession rate. In general, all material candidates showed significantly lower peak backface temperatures when compared with PICA, and both PhenCarb 28/15 and BPA-FG show a recession rate about half that of PICA at this heating condition.

Figures 19 and 20 show the recession rate and peak backface temperature results for the test articles at the higher heating condition. MonA-18 backface temperature data was not included since it was tested at a reduced duration. In this case, a significant correlation between recession and density were not observed. As with the lower heating condition, Graded MonA shows excellent insulative properties along with the highest recession rate. At this condition, peak backface temperatures ranged from 60 to 80 °C for the material candidates and were again significantly lower than PICA.

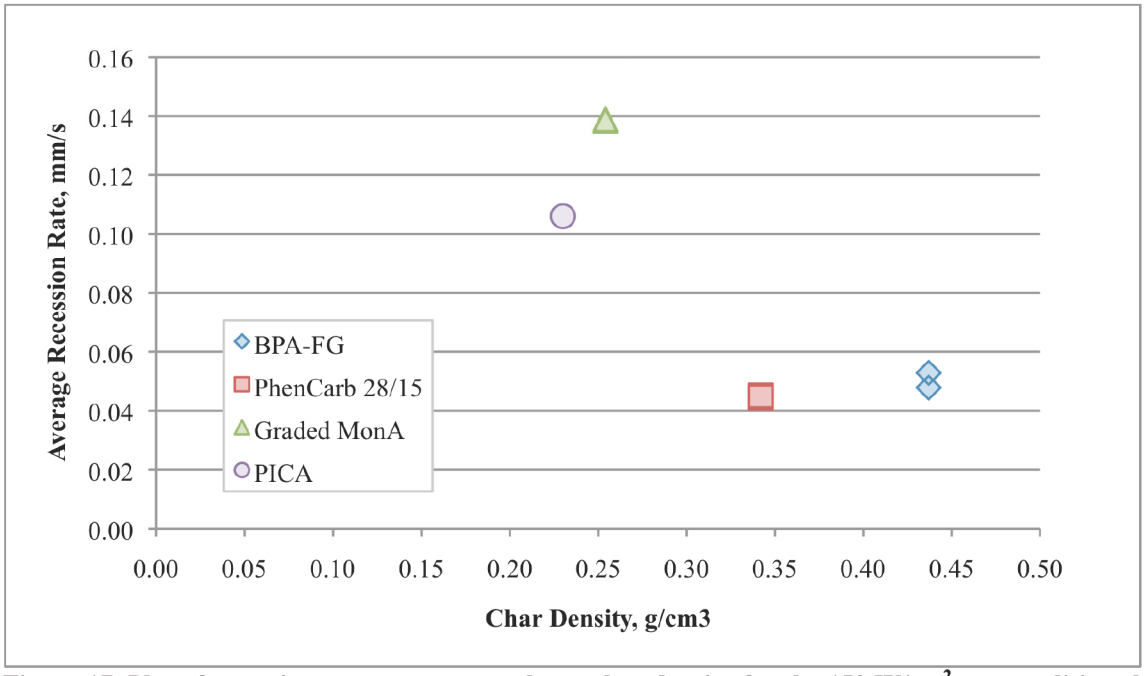

Figure 17. Plot of recession rate versus outer layer char density for the 150 W/cm^2 test condition showing an inverse correlation.

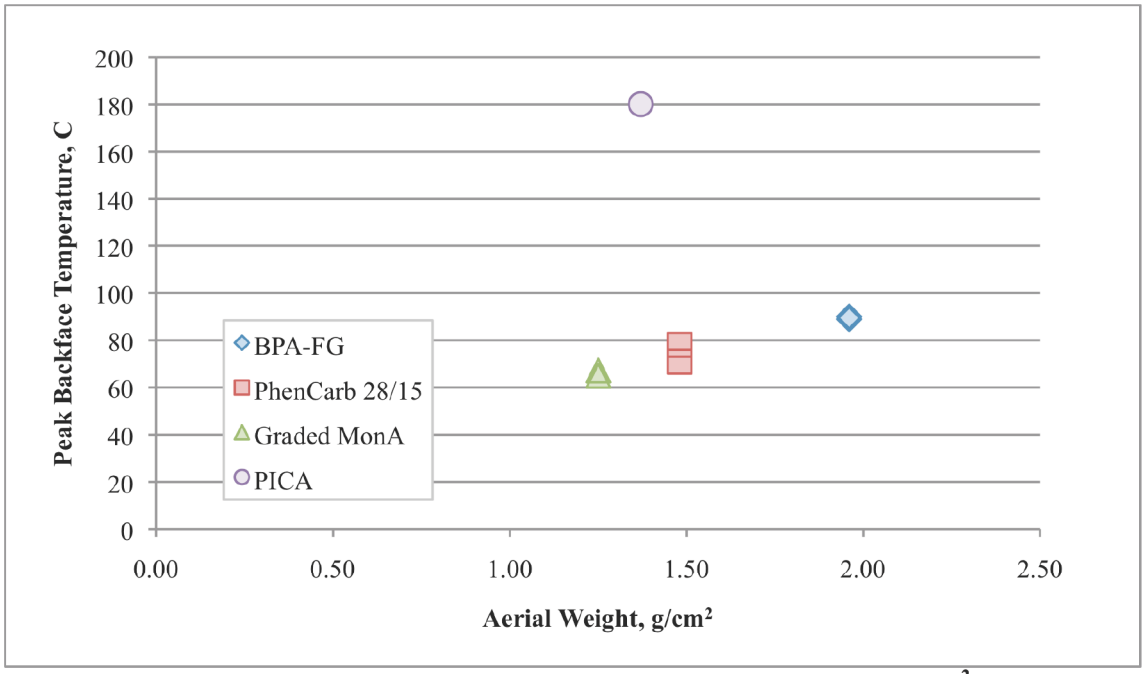

Figure 18. Plot of peak backface temperature versus aerial weight for the 150 W/cm^2 test condition showing a correlation for all materials except PICA (which has significantly higher thermal conductivity).

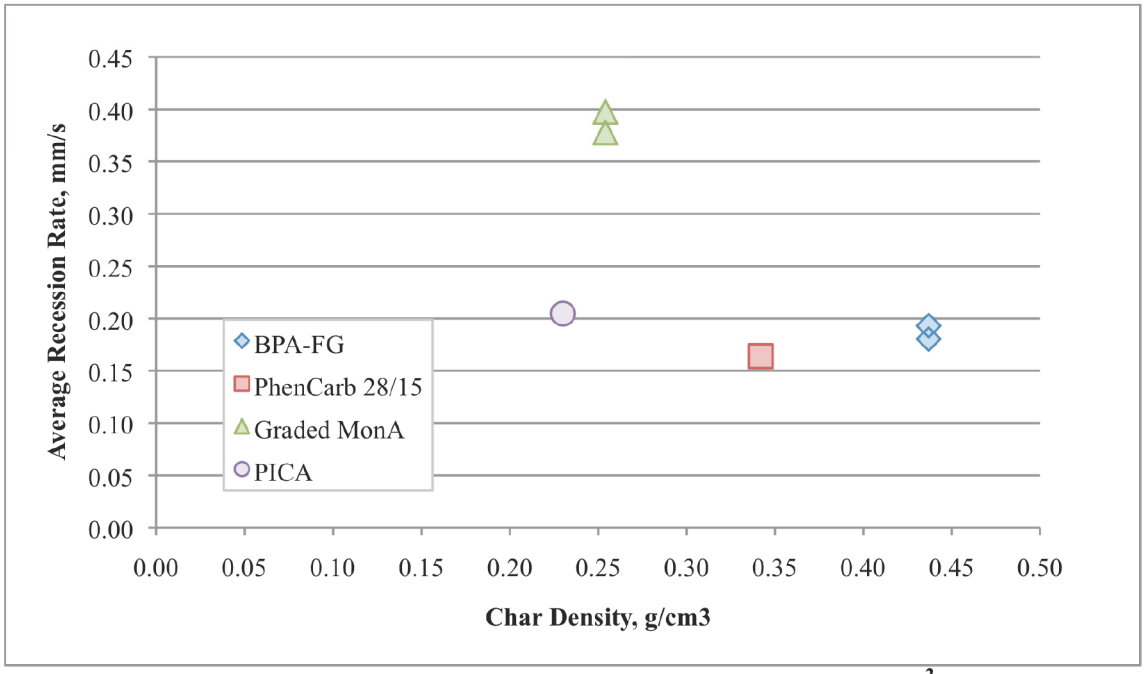

Figure 19. Plot of recession rate versus outer layer char density for the 450 W/cm^2 test condition.

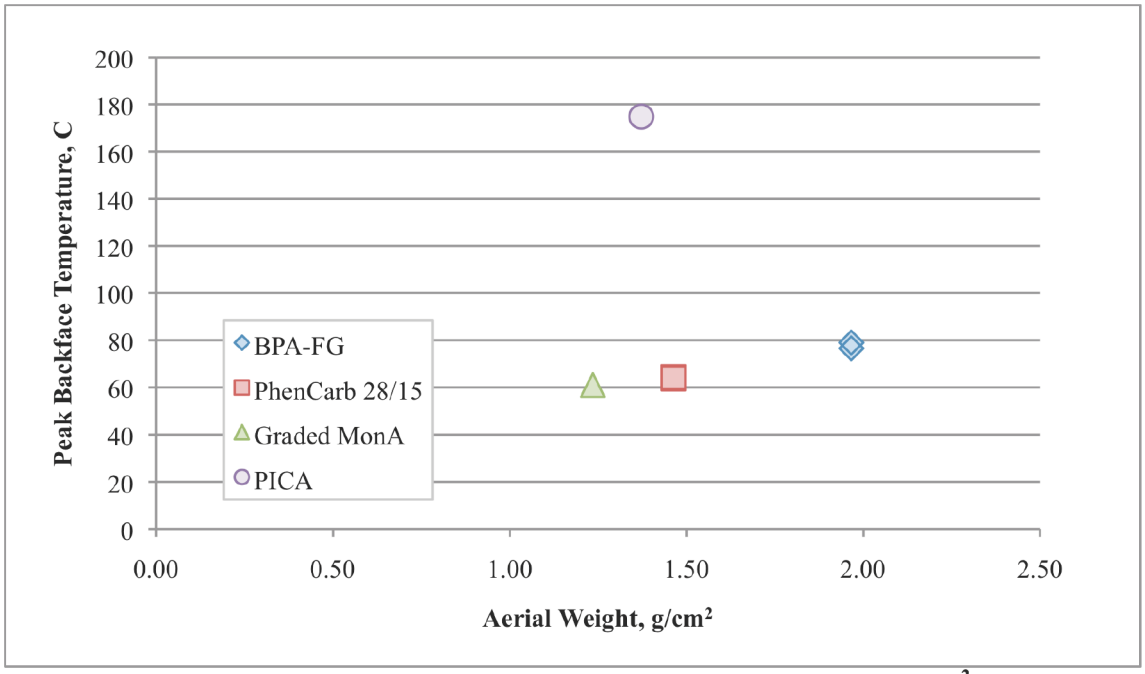

Figure 20. Plot of peak backface temperature versus aerial weight for the 450 W/cm^2 test condition showing a correlation for all materials except PICA (which has significantly higher thermal conductivity).

V. Summary

The increased demand on thermal protection system performance from current and future Mars missions has motivated the development of superior ablative TPS. This paper describes NASA's efforts, under the EDL Technology Development Project, to test the performance and characterize the properties of materials from industry partners. Boeing's BPA-FG, Applied Research Associate's PhenCarb 28/15, and Lockheed's Graded MonA were all tested under this project and show promise.

A full set of thermal property data was obtained for the three dual layer systems. This data, coupled with in-depth temperature response during arcjet testing, will facilitate thermal and ablation response modeling of these advanced ablators. All three systems show significantly superior insulative capabilities compared to the state-of-the-art material PICA, with the same or modestly higher system densities. Thermal conductivity testing, which is challenging to accurately perform on porous ablative materials, was carried out in four different facilities giving reasonable reproducibility.

A new three-point bend test configuration was developed to address the concern of dual layer ablator having low interface strength. The substrate was designed with stress relief cuts and varying thickness to reduce the chance of failure at the ends of the ablator block and increase the shear and tension stresses in the middle of the ablator block. BPA-FG showed the highest stiffness while PhenCarb reached the highest level of strain at failure. Billet inspection and specimen fabrication revealed some structural shortcomings, such as voids or cracks, for all of the tested materials that will need to be addressed with further development of these ablators.

Tensile testing showed that all three systems have good interface adhesion between layers, and that TTT strengths were much higher than that for state-of-the-art PICA. In-plane strengths of BPA-HD and PhenCarb-28 were very high, while the strength of PhenCarb-15 was moderate and that of BPA-LD was quite low. Both MonA layers had low in-plane strengths due to pre-existing cracks observed upon billet inspection. Notably, none of the new materials met the EDL TDP goal of significantly increasing the strain-to-failure capability beyond that of PICA.

A developmental arc jet test series of three rigid ablative materials was completed in the ARMSEF arc jet test facility at NASA Johnson Space Center. All articles survived the test conditions, and mass loss, recession, and surface and backface thermal response data were obtained, thus successfully meeting test objectives. In general, Graded MonA (at the lowest areal weight) showed the highest recession, but peak backface temperatures significantly lower than PICA. At the lower heating condition, PhenCarb 28/15 and BPA-FG showed about half the recession rate of PICA, but at the higher heating rate had a similar recession rate to PICA. General ablative efficiency of all materials was demonstrated with similar peak backface temperatures at the higher heating condition, when compared to the lower heating condition, even though the higher condition had a heat load double that of the lower condition. Ablative and thermal response data was obtained for all material candidates in an air environment. Tests in carbon dioxide are on-going and will be presented in a subsequent report. The data obtained from this test series can be utilized in the development of thermal response models for these new ablative materials.

Acknowledgments

This work was supported by the Entry, Descent, and Landing Technology Development Project: Michael Wright (EDL TDP Principle Investigator, NASA Ames) and Michelle Munk (EDL TDP Project Manager, NASA LaRC). The authors gratefully acknowledge the support provided by the Thermal Protection Materials Branch of NASA Ames Research Center and NASA Contract No. NNA10DE12C with the ERC Corporation. Portions of this work were carried out by the Jet Propulsion Laboratory, California Institute of Technology, under a contract with the National Aeronautics and Space Administration.

The authors greatly appreciate the assistance of Mike Fowler (JSC) and Jeremy Thornton (ARC) in helping to gather physical properties of the respective TPS materials. T. Gökçen (ARC) provided arcjet environment simulations. FWT tests were performed by Keith Bird and Stewart Walker. Arcjet testing was performed at NASA JSC with the support of Stan Bouslog, Brian Remark, Scott Coughlin and Steve DelPapa. Antonella Alunni (ARC) assisted with material property data analysis, and Ethan Post (JPL) provided assistance with arcjet data reduction. In addition, there was significant support at NASA Ames Research Center for test article design (Jose Chavez-Garcia) and fabrication (Matt Switzer and Don Ebaugh).

References

[1]Cassell, A. M., Beck, R. A. S., Arnold, J. O., Hwang, H., Wright, M. J., Szalai, C. E., Blosser, M., Poteet, C. C., "Development of Thermal Protection Materials for Future Mars Entry, Descent and Landing Systems," AIAA 2010-5049, 10th AIAA/ASME Joint Thermophysics and Heat Transfer Conference, 28 June – 1 July 2010, Chicago, Illinois.

[2]M. Munk (LaRC) "Overview of the NASA Entry, Descent and Landing Systems Analysis (EDL-SA)," 7th International Planetary Probe Workshop, Barcelona, Spain, June 2010.

[3]Chen, Y.-K., and Milos, F. S., "Ablation and Thermal Response Program for Sapcecraft Heatshield Analysis," AIAA Paper No. 98-0273, 1997.

[4]Milos, F. S., and Chen, Y.-K., "Ablation and Thermal Response Property Model Validation for Phenolic Impregnated Carbon Ablator," *Journal of Spacecraft and Rockets,* Vol. 47, No. 5, 2010, pp 786-805.

[5]Chen, Y.-K., Milos, F. S., and Gokcen, T., "Validation of a Three-Dimensional Ablation and Thermal Response Simulation Code," AIAA Paper No. 2010-4645, June 2010.

[6]Wright, M. J., Beck, R. A. S., Edquist, K. T., Driver, D., Sepka, S. A., Slimko, E. M., Wilcockson, W. H., DeCaro, A., and Hwang, H. H., "Sizing and Margins Assessment of the Mars Science Laboratory Aeroshell Thermal Protection System," AIAA Paper No. 2009-4231, June 2009.

[7]Cozmuta, I., Wright, M. J., Laub, B., and Willcockson, W. H., "Defining Ablative Thermal Protection System Margins for Planetary Entry Vehicles," AIAA Paper No. 2011-3757, June 2011.

[8]Sepka, S. A., and Wright, M. J., "Monte Carlo Approach to FIAT Uncertainties with Applications for Mars Science Laboratory," *Journal of Thermophysics and Heat Transfer,"* Vol. 25, No. 4, 2011, pp 516-522.

[9]Feldman, J., Alunni, A., and Stackpoole, S., "Thermal and Mechanical Property Testing Orion Heat Shield Candidates," 34th Annual Conference on Composites, Materials, and Structures (ITAR Session), 25-28 January 2010, Cocoa Beach, FL.

[10]Feldman, J., Alunni, A., Sepka, S., Stackpoole, M., Bird, K., Fowler, M., and Ellerby, D., "Material Properties of PICA," NASA TM 2010-216399, 2010.

[11]Rooke, S. P., and Taylor, R. E., "Transient Experimental Technique for the Determination of the Thermal Diffusivity of Fibrous Insulation, " *Journal of Heat Transfer (Transactions of the ASME, Series C),* 1988, pp 270-273.

[12]Larin, M., Marichalar, J., Kinder, G., Campbell, C., Riccio, J., Nguyen, T., Del Papa, S., and Pulsonetti, M., "Boundary Layer Transition Protuberance Tests at NASA JSC Arc-Jet Facility," AIAA 2010-1578, 48th AIAA Aerospace Sciences Meeting Including the New Horizons Forum and Aerospace Exposition, 4-7 January 2010, Orlando, Florida.